

# Formation and interaction of hydrated alkali metal ions at the graphite-water interface

Sheng Meng<sup>a)</sup>

Department of Physics, Harvard University, Cambridge, Massachusetts 02138  
and Condensed Matter Sciences Division, Oak Ridge National Laboratory,  
Oak Ridge, Tennessee 37831

Shiwu Gao

Department of Applied Physics, Chalmers University of Technology and Göteborg University,  
SE4-12 96 Göteborg, Sweden and Institute of Physics, Chinese Academy of Sciences,  
10080 Beijing, People's Republic of China

(Received 28 February 2006; accepted 25 April 2006; published online 6 July 2006)

Ion hydration at a solid surface ubiquitously exists in nature and plays important roles in many natural processes and technological applications. Aiming at obtaining a microscopic insight into the formation of such systems and interactions therein, we have investigated the hydration of alkali metal ions at a prototype surface-graphite (0001), using first-principles molecular dynamics simulations. At low water coverage, the alkali metal ions form two-dimensional hydration shells accommodating at most four (Li, Na) and three (K, Rb, Cs) waters in the first shell. These two-dimensional shells generally evolve into three-dimensional structures at higher water coverage, due to the competition between hydration and ion-surface interactions. Exceptionally K was found to reside at the graphite-water interface for water coverages up to bulk water limit, where it forms an “umbrellalike” *surface hydration shell* with an average water-ion-surface angle of 115°. Interactions between the hydrated K and Na ions at the interface have also been studied. Water molecules seem to mediate an effective ion-ion interaction, which favors the aggregation of Na ions but prevents nucleation of K. These results agree with experimental observations in electron energy loss spectroscopy, desorption spectroscopy, and work function measurement. In addition, the sensitive dependence of charge transfer on dynamical structure evolution during the hydration process, implies the necessity to describe surface ion hydration from electronic structure calculations. © 2006 American Institute of Physics. [DOI: 10.1063/1.2206591]

## I. INTRODUCTION

Ions at the surfaces and interfaces in contact with water present in many natural phenomena such as solvation, wetting, corrosion, gas release, neural signal transport, and enzyme regulation, as well as in a lot of technological applications including electrolysis and catalysis.<sup>1-4</sup> On a real surface, water molecules and common ions are hardly avoidable.<sup>5</sup> The interaction between them is always involved with the substrate, making the surface phenomena even more complicated. Consequently, the hydrated ions play crucial roles in determining the physical, chemical, electrical, and mechanical properties of surfaces, e.g., surface morphology, catalytic property, conductivity, and wettability.<sup>1,2</sup> In particular, hydrated ion binding at the surface of biomolecules (proteins and DNA) and at the outer mouth of ion channels, is very important for biological signal recognition, the selectivity of ions, biosensors, and drug design.<sup>6</sup>

In aqueous solutions, it is well known water molecules around the ion form a three dimensional (3D) shell-like structure, the so-called hydration shell (HS).<sup>7</sup> The first HS comprises three to nine waters which are directly chemically bonded to the ion, while the second and later hydration shells

are maintained by both the hydrogen bonding to the first shell and the long-ranged electrostatic attraction of the ion.<sup>8</sup> The same concept applies to nanometer ion-water clusters. However, it is not clear how these structures would change when they approach an interface. Limited number of studies have been focused on alkali metal (AM) ion hydration at metal surfaces,<sup>9</sup> graphite,<sup>10,11</sup> and mica.<sup>12,13</sup> While current experimental techniques meet great challenges in measuring the structures in the highly disordered, inhomogeneous interfacial region, due to the complications introduced by the broken symmetry and charge transfer, it is relatively straightforward to predict structures, kinetics, and dynamics properties of surface-bound ion HS using computer simulations on the *molecular level*. It has been shown successful in describing solid-water interface<sup>14</sup> and ion hydration in solutions<sup>15</sup> recently.

We have studied the hydrated AM cation on graphite due to its simplicity and the available experimental data, using state-of-the-art *ab initio* molecular dynamics (MD) simulations. Graphite is a softly layered biomimetic material, but still represents a well-characterized solid surface with fascinating properties such as half-metallic and hydrophobic. In a previous study, we have employed vibrational recognition to identify hydrated K and Na ions, which form two-dimensional (2D) hydration shells on graphite surface at low

<sup>a)</sup>Electronic mail: shmeng@deas.harvard.edu

water coverage.<sup>16</sup> Here we report our new study with significant extensions. First, we include five alkali metals, Li, K, Na, Rb, and Cs, for a complete comparison and general trend. Second, we extend the study of ion-water clusters to the hydration shell in the presence of bulk liquid water at the water/solid interface. Third, the interaction between hydrated ions at the interface is studied, at various water coverages and cation concentrations. Questions concerning geometrical confinement of the 2D surface, formation of 2D ion hydration shells, general trends for different ions, ion dynamics at low water coverage up to bulk water limit, and ion-ion interaction in the water medium, are addressed in the present work. The finding of the 2D hydration shell of all AM ions on graphite agrees with experimental electron energy loss spectra (EELS).<sup>10</sup> The intriguing competition between hydration and ion-surface interactions at higher water coverages which leads to dissolution of Na and surface HS of K, the water-mediated ion-ion interaction that favors Na ions aggregation and Li, K, Rb, and Cs separations, and work function change upon electron transfer between adsorbates and the graphite surface, again agree with experimental temperature programmed desorption (TPD) measurements and work function data.<sup>11,17,18</sup>

The rest of this paper is organized as follows. We first present in Sec. II the methods and computational details we used, and the systematical check on their validity. Then in Sec. III we present our main results and discussion. Topics include, (i) the bare ion adsorption and (ii) the hydration shell formation of a single alkali metal, including Li, Na, K, Rb, and Cs, on graphite (0001) at low water coverage; (iii) multi-ion hydration and ion-ion interaction mediated by water; (iv) charge transfer as well as work function changes involved in the ion hydration process; and (v) surface hydration dynamics at bulk water/graphite interface. Finally a brief summary is given in Sec. IV.

## II. METHODS

The first-principles calculations were performed with the Vienna *ab initio* simulation program,<sup>19</sup> in the framework of density functional theory (DFT). The supercell with periodic boundary condition consists of one layer of graphite sheet in a  $4 \times 4$  unitcell (separated by at least 17 Å), several adsorbed AM atoms, and  $n$  H<sub>2</sub>O molecules where  $n=1-10$  for clusters, and  $n=37$  for the bulk water limit. The latter corresponds to a density of  $\sim 1$  g/cm<sup>-3</sup> for water confined between two adjacent graphite sheets. The adsorbed ions and water molecules were put on one side of the slab. For a single AM ion adsorption, this supercell corresponds to an ion coverage of  $1.2 \times 10^{14}$  atoms/cm<sup>2</sup>, and the coverage is two to four times higher if there are two to four AM atoms presented in the supercell. These coverages are comparable to that in the experiment<sup>10</sup> ( $0.5-5.4 \times 10^{14}$  atoms/cm<sup>2</sup>).

A cutoff of 300 eV in planewave basis and a  $3 \times 3 \times 1$   $k$ -point sampling were used. Gaussian smearing at the Fermi level with a width of 0.1 eV was employed. The free energy was extrapolated to zero Kelvin to yield total energies of the systems. This set of parameters assures a convergence of 0.01 eV/atom in total energy. Usually the hydrated structures

were determined by *ab initio* MD simulations from many different starting configurations. The energetics were extracted by further relaxation until the forces on every atom which is allowed to relax are less than 0.05 eV/Å. Spin-polarized calculations are not necessary because the adsorption systems have zero magnetic moment.

In structural search, the AM ions and water molecules were relaxed simultaneously, while the surface graphite layer was fixed. Calculations with the graphene sheet fully relaxed show minor changes in structures and energetics. For example, the change in bond lengths is 0.01 Å for Li-O and 0.05 Å for C-Li, and the change in total energy is as small as 0.001 eV/atom for (Li+H<sub>2</sub>O)/graphite. In MD simulations, the AM ion and water molecules were allowed to move according to the forces calculated from the converged electronic structure, employing the Born-Oppenheimer approximation. A time step of 0.5 fs was utilized in all MD simulations. The trajectories were collected through a 4 ps production run at 85 K (for water clusters) and 300 K (for bulk water) after equilibrating the system for  $\sim 1$  ps.

The adsorption energy of the AM atoms on the graphite surface is defined by the energy difference between the AM/graphite system and those for separated graphite and free AM atoms.

$$E_{\text{ads}} = \{E[\text{graphite}] + m \times E[\text{AM}] - E[m(\text{AM})/\text{graphite}]\}/m, \quad (1)$$

where  $E$  is the total energy of the graphite, the free AM atom, and the whole adsorption system, respectively, and  $m$  is the number of AM atoms in the supercell. The hydration energy of AM ions in a surface hydration shell,  $E_h$ , is defined as the mean adsorption energy per H<sub>2</sub>O in the AM+water/graphite system,

$$E_h = \{E[\text{AM}/\text{graphite}] + n \times E[\text{H}_2\text{O}] - E[(n\text{H}_2\text{O} + \text{AM})/\text{graphite}]\}/n. \quad (2)$$

Here  $E$  is the total energy of the AM/graphite, the free H<sub>2</sub>O molecule, and the hydration system, respectively, and  $n$  is the number of water molecules in the supercell.

We used Vanderbilt ultrasoft pseudopotentials<sup>20</sup> (USPP) for electron interaction with the ion nuclei, and the PW91 form of exchange-correlation (XC) energy.<sup>21</sup> Semicore  $p$  electrons are treated as valence electrons. Nonlinear core corrections are included in the USPP for AM atoms. It has been shown that the projector augmented wave (PAW) method<sup>22</sup> has improved accuracy, especially for calculations of alkali metals. Our comparison with PAW calculations shows negligible structural difference (within 1%) while the energy might shift slightly for AM adsorption on graphite (Table I). The general gradient approximation (GGA) in XC functional is crucial for accurate treatment of the hydrogen bonds in water structures and charge transfer effects which are critical in present calculations. Extensive comparison between different GGA functionals shows that PW91 [and its derivative Perdew-Burke-Ernzerhof<sup>23</sup> (PBE)] has been the most promising for describing the hydrogen bonding,<sup>24</sup> bulk ice,<sup>25</sup> and liquid water.<sup>26</sup> In particular, it has been shown to be very successful at surfaces.<sup>27</sup> For example, the PW91/

TABLE I. Adsorption heights ( $z_{AM}$ ) and energies ( $E_{ads}$ ) for AM=Li, Na, K, Rb, and Cs on graphite (0001) surface. Adsorption on bridge sites has very similar energies and heights as on top sites and is not listed. Numbers in parenthesis are results from PAW-PBE calculations.

	Hollow		Top	
	$z_{AM}$ (Å)	$E_{ads}$ (eV)	$z_{AM}$ (Å)	$E_{ads}$ (eV)
Li/graphite	1.69 (1.71)	1.34 (1.28)	2.01 (2.05)	1.04 (0.99)
Na/graphite	2.38 (2.40)	0.75 (0.69)	2.62 (2.62)	0.70 (0.65)
K/graphite	2.70 (2.70)	1.01 (0.95)	2.83 (2.85)	0.95 (0.89)
Rb/graphite	2.87	0.96	2.99	0.92
Cs/graphite	3.22	0.97	3.33	0.94

PBE gives a much smaller mean error (ca. 5%) to the XC energy of surfaces than other commonly used functionals, such as the BLYP functional, whose mean error is seven times larger.<sup>27</sup> For the treatment of surface ion HS, we compared these different XC functionals in a prototype case of Na coadsorbed with a water molecule in Table II, where they show negligible differences in bond lengths and water orientation but a small difference in hydration energies (0.02–0.03 eV). The reported structure and energy for Li/graphite (1.71 Å and 1.36 eV) using more accurate B3LYP functional<sup>28</sup> also compare very nicely with our result.

The much weaker interlayer van der Waals (vdW) coupling of graphite [35 meV (Ref. 29)] is neglected. It has been shown the difference of K adsorption on single-layered graphite and multilayer graphite is negligible.<sup>30</sup> We would like to point out here that the fundamental interaction involved in the hydration at the graphite surface is primarily the ionic interaction rather than the weak vdW forces, which are essential in the water-(bare)graphite interaction (ca. 0.16 eV for monomer/graphite<sup>31</sup>) as well as interlayer coupling of bulk graphite. This is due to the ionization of the alkali atoms by the surface, leads to a positively charged ion and a negatively charged surface (the so-called electric double layer). The latter in turn results in strong ionic interactions between the ion and surface (0.7–1.3 eV), and between the ion and water molecules (0.5–0.8 eV). The dipole-dipole interaction between the supercell and its images due to the periodic boundary condition is small. For example, the dipole interaction energy between adjacent adsorbate-graphite layer is 0.021 eV for K+5H<sub>2</sub>O/graphite. Whenever this dipole interaction appears large, the separation between adjacent graphite layers is increased to 30 Å to reduce prominent artificial effects due to the finite size of

supercell. Moreover, this intercellular dipole-dipole interaction does not contribute to the hydration energy, which is intracellular.

### III. RESULTS AND DISCUSSION

#### A. Adsorption and ionization of alkali atoms on graphite

Before studying the hydration process, we have calculated the adsorption of bare alkali metal atoms including Li, Na, K, Rb, and Cs on graphite (0001) surface. The heights and binding energies at the top and hollow sites are given in Table I. As bridge sites adsorption has very similar energies (difference < 0.01 eV) and bond lengths (< 0.04 Å) as on top sites, they are omitted in the table. The numbers in the parenthesis are results from more accurate PAW calculations using PBE exchange-correlation functional, which agree with the USPP-PW91 result very well. All AM atoms prefer to adsorb at the hollow site. This result seems to be a general feature of alkali metal atoms on graphite and carbon nanotubes.<sup>32</sup> The energy difference between the two adsorption sites diminishes as the atomic number increases. It is the largest for Li (0.30 eV), but almost negligible for Cs (0.03 eV). The adsorption energy does not show a monotonic variation with the atomic number. In particular, the Na atom has a substantially lower binding energy (0.75 eV) compared with other atoms. The adsorption height, on the other hand, increases gradually from Li to Cs. It can be attributed to the gradual increase of their ionic radii. The nonmonotonic behavior in the adsorption energy indicates that intrigue interaction beyond the simple picture of ionicity of AM atoms may be operative in the AM-graphite systems.

In order to understand the bonding nature of AM atoms on graphite, the density of states (DOS) for graphite (0001) surface and the projected DOS for the *s* electrons of adsorbed K and Na, as specific examples, are plotted in Fig. 1. As commonly observed, the graphite has a semimetal behavior whose DOS shows a minimum of zero at the Fermi level. Upon adsorption, both K 4*s* and Na 3*s* orbitals lie dominantly above the Fermi level, indicating a significant electron donation (approximately 0.7 electron) from K or Na to the graphite surface. In addition, the K 4*s* orbit is shifted 0.1 eV further above the Fermi energy than Na 3*s* to deplete more electrons, indicating K is further ionized than Na, a consequence of larger polarizability of the former. The DOS for other AM atoms has the same feature, i.e., all of them have an *s* orbit greatly depleted right above Fermi energy. Therefore an adsorbed AM atom is largely ionized upon adsorption

TABLE II. Comparison between different exchange-correlation functionals for a prototype system of a Na and a water molecule coadsorbed on graphite (0001). The adsorption height of Na, the ONa and OH bond lengths, the bond angles, and the water hydration energy (in units of angstrom, degree, and eV) are compared.  $\angle\text{NaOH}'$  and  $\angle\text{HOH}$  is the angle the ONa bond makes to the water plane and the internal water binding angle, respectively.

Functional	$z_{Na}$	$d_{ONa}$	$\angle\text{NaOH}'$	$d_{OH}$	$\angle\text{HOH}$	$E_h$
PW91	2.378	2.337	127.69	0.978	103.92	0.70
PBE	2.372	2.357	126.63	0.986	103.63	0.73
BLYP	2.387	2.353	129.16	0.987	103.84	0.68

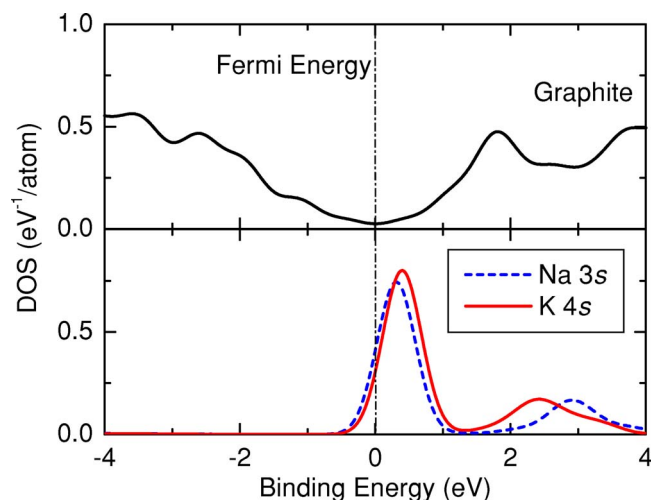


FIG. 1. (Color online) Upper panel, the density of states (DOS) of graphite (0001) surface; lower panel, projected DOS for the  $s$  electrons of adsorbed K and Na on graphite. The dot-dashed line indicates the Fermi level.

on graphite, forming strong ionic AM-graphite bonds. This conclusion is consistent with the measured x-ray adsorption spectrum of K/graphite.<sup>33</sup> The ionized electron is distributed mainly in a narrow region between the ion and the atomic plane of graphite, as shown by the plane-averaged charge density of the transferred K 4s and Na 3s electrons in Fig. 2. The center of the graphite sheet is positively charged, while two maxima of electron density locate at  $z=0.85$  Å and  $z=-0.42$  Å from the surface, respectively. Here the direction  $z$  is the surface normal. Detailed analysis suggests that the ionized electron is populated in the hybridized  $s+p_z$  state on the six neighboring carbon atoms. This can be clearly seen from the 2D charge distribution in the  $z=0.85$  Å plane as shown in Fig. 3. Other AM atoms also show qualitatively the same picture.

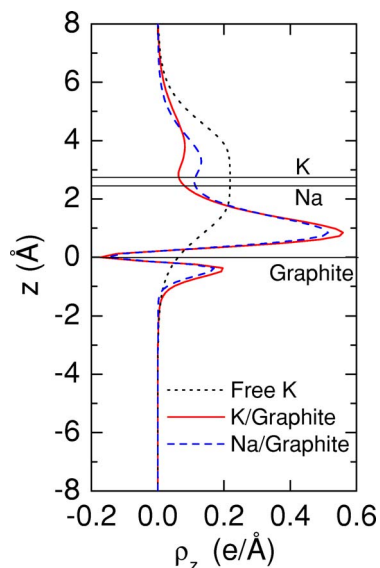


FIG. 2. (Color online) Planar averaged charge distribution of the K 4s and Na 3s valence electrons along the surface normal ( $z$  direction), upon their adsorption on graphite. The charge density is calculated from the density difference between K(Na)/graphite and free graphite (only  $s$  electrons are treated as valence for K and Na). Charge around a free K atom is also shown as the dotted line. The positions of K (Na) and the graphite surface are indicated by horizontal lines.

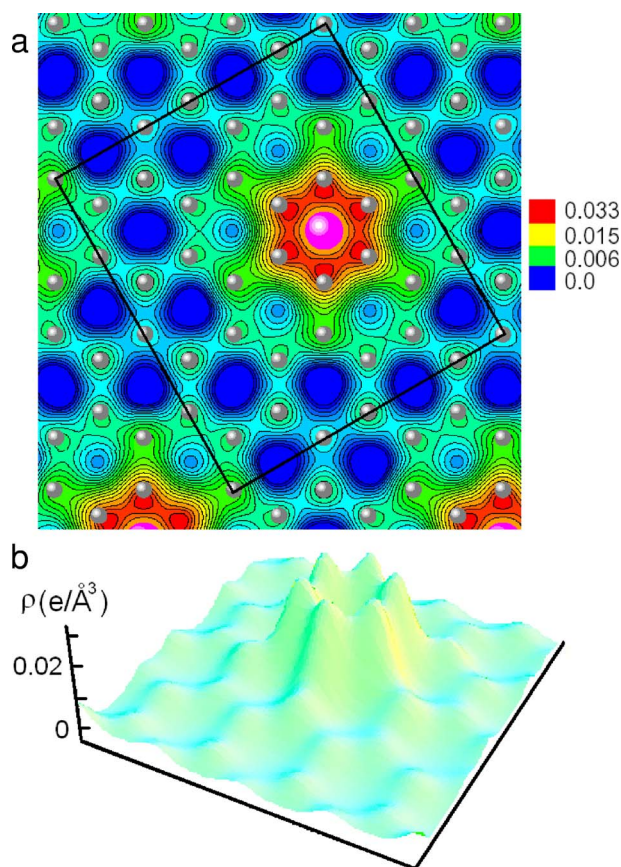


FIG. 3. (Color online) (a) Top view and (b) side view of two-dimensional charge distribution in the plane  $0.85$  Å above the graphite surface for K/graphite. Small (big) balls represent the atom positions of C (K) projected on the plane.

The calculated results compare well with available experiments and other calculations. For example, the adsorption energies of K (1.01 eV) and Na (0.75 eV) in Table I agree well with the measured values of 1.15 eV (K) and 0.77 eV (Na),<sup>10,11</sup> respectively. Early calculations using B3LYP functional and finite graphite sheet also gave an adsorption energy of 1.36 eV (1.09 eV) and height of 1.71 Å (2.03 Å) for Li at the hollow (top) site,<sup>28</sup> which are in good agreement with our results in Table I. Such comparisons justify the validity of our approach in the treatment of AM atoms on graphite surface.

## B. Hydration shells at low water coverage

In the previous study,<sup>16</sup> the hydration structure of the K ion and water was studied in detail. Here we extend this study to other AM ions.

As found in the previous study,<sup>16</sup> the microscopic structures of  $K+nH_2O$ , with  $n=1-10$ , can be categorized by three types. Type I,  $n \leq 3$ , the first hydration shell; Type II,  $4 \leq n \leq 6$ , the second hydration shell in 2D; and Type III,  $n \geq 7$ , three-dimensional shell structure. These structures are depicted in Fig. 4 in detail. Different from the case in free clusters, the shell structures are strongly modified by the presence of the surface, which breaks the symmetry of the shells mechanically and polarizes the electronic distribution of the shells through the ionized charge on the graphite sheet.

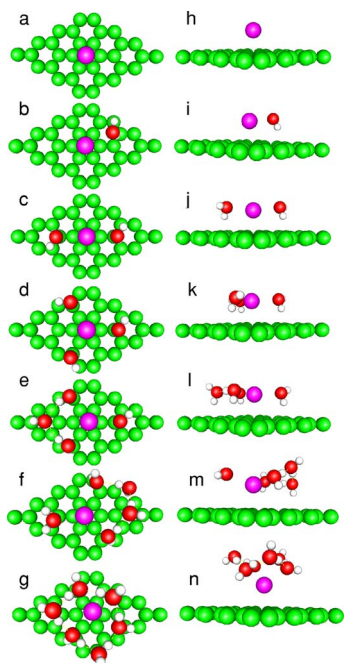


FIG. 4. (Color online) The 2D hydration structures for K and  $K+nH_2O$ ,  $n=1-6$ , on the graphite surface. (a)–(g) Top views; (h)–(n) side views.

Similar to the K case, the shell structures for other AM  $+nH_2O$ /graphite can also be divided into three types: (i) the first hydration shells at  $n=1-4$  for Li and Na, and  $n=1-2$  for Rb and Cs; (ii) the second 2D shells at  $n=3-6$ , and (iii) the bulk water limit at larger  $n$ . The details of these hydration structures are summarized in Table III. In particular, most of these hydration shells exhibit a rather flat structure or compressed tetrahedral structure. The  $H_2O$  molecules in first shell are at approximately the same height as the AM ion

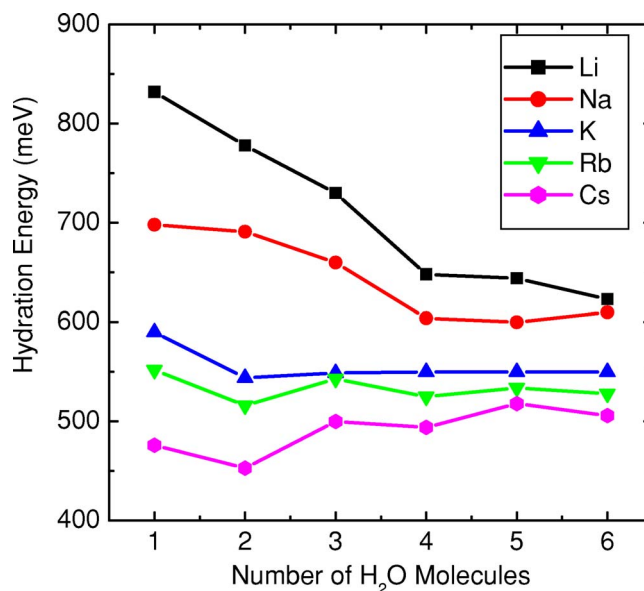


FIG. 5. (Color online) Hydration energy as a function of the number of  $H_2O$  molecules in the most stable hydration structures for Li, Na, K, Rb, and Cs on graphite.

above the surface. The averaged O–M bond length,  $d_{OM}$ , increases from Li to Cs: 2.039 Å (Li), 2.338 Å (Na), 2.819 Å (K), 2.880 Å (Rb), and 3.215 Å (Cs). The adsorption height of the ion (and its HS) increases with increasing AM ion radii and water coverage. The trends in bond length and adsorption height can be understood from the ionic radii of AM atoms and the energetics of hydration discussed below.

The calculated hydration energies for the AM ions are shown in Fig. 5 for  $n$  up to 6. Two general features can be found. First, the hydration energy decreases as the atomic

TABLE III. The most stable hydration shell structures and their hydration energies ( $E_h$ ), for alkali metals (AM=Li, Na, K, Rb, and Cs) coadsorbed with  $n H_2O$  on graphite (0001), with  $n=1-6$ . Here  $z_{AM}$  is the adsorption heights of the ion above the surface, and  $n_1+n_2$  specifies the number of water molecules in the first ( $n_1$ ) and second ( $n_2$ ) shell at a given number of waters  $n=n_1+n_2$ . Energies and distances are in eV and angstrom, respectively.

$n$	1	2	3	4	5	6
$E_h$ [Li]	0.83	0.78	0.73	0.65	0.64	0.62
$z_{AM}$	1.861	2.073	2.670	2.923	3.334	2.407
$n_1+n_2$	1+0	2+0	3+0	4+0	4+1	3+3
$E_h$ [Na] <sup>a</sup>	0.70	0.69	0.66	0.60	0.60	0.61
$z_{AM}$	2.614	2.658	4.019	4.680	5.162	5.559
$n_1+n_2$	1+0	2+0	3+0	4+0	4+1	4+2, 3+3
$E_h$ [K] <sup>a</sup>	0.59	0.54	0.55	0.55	0.55	0.55
$z_{AM}$	3.026	3.011	3.210	3.325	3.390	3.136
$n_1+n_2$	1+0	2+0	3+0	3+1	3+2	3+3
$E_h$ [Rb]	0.55	0.52	0.54	0.53	0.53	0.53
$z_{AM}$	2.920	2.997	2.994	3.118	3.201	2.932
$n_1+n_2$	1+0	2+0	2+1	3+1	3+2	3+3
$E_h$ [Cs]	0.48	0.45	0.50	0.49	0.52	0.51
$z_{AM}$	3.265	3.310	3.331	3.470	3.439	3.302
$n_1+n_2$	1+0	2+0	2+1	3+1	3+2	3+3

<sup>a</sup>From MD simulations at 85 K.

TABLE IV. Adsorption energy (in eV/ion) and structural parameters (ion-surface distances and ion-ion distances, in angstrom) for multi-ion adsorption on graphite. "S" refers to "Surface."

	$n$	1	2	3	4
$n\text{K}/\text{Graphite}$	$E_{\text{ads}}$	1.006	0.859	0.900	0.928
	$d_{\text{K-S}}$	2.698	2.975	3.147	3.208
	$d_{\text{K-K}}$	...	4.903	4.598	4.942
$n\text{Na}/\text{Graphite}$	$E_{\text{ads}}$	0.748	0.797	0.910	0.889
	$d_{\text{Na-S}}$	2.380	2.963	2.701	3.067
	$d_{\text{Na-Na}}$	...	3.269	3.359	3.686

number increases from Li to Cs. It is the strongest for Li ion, 0.83 eV for single  $\text{H}_2\text{O}$ . However, it is still much less than that in bulk water, 1.42 eV.<sup>34</sup> Second, the hydration energy for all species seems to converge to each other as more  $\text{H}_2\text{O}$  molecules are added to the hydration shells. For example, the hydration energy for Li decreases from 0.83 eV for Li +  $1\text{H}_2\text{O}$  to 0.62 eV for Li +  $6\text{H}_2\text{O}$ . In contrast, it increases from 0.45 eV (Cs +  $2\text{H}_2\text{O}$ ) to 0.51 eV (Cs +  $6\text{H}_2\text{O}$ ). The changes in hydration energy results from the gradual transition from the ion-water interaction to the interwater H bonding. This feature is reasonable because the hydration energy of the ions, defined as the averaged energy gain per  $\text{H}_2\text{O}$  in the hydration structures, should approach the cohesive energy of the bulk water when more  $\text{H}_2\text{O}$  molecules are placed around the ions.

It is interesting to note two specific characters of the 2D hydration shells. (i) For all AM a relatively stable hydration shell forms at  $n=6$ , which has a hexagonal geometry with three lower-lying water molecules directly bound to the AM, and the other three upper  $\text{H}_2\text{O}$  connected to the first shell by hydrogen bonds alternatively ("3+3"), thus forming an umbrella-like structure [Figs. 4(g)–4(n)]. It resembles the hexagonal building block of the naturally occurring bulk ice Ih, which results in its particular stability. (ii) At  $n=2$ , the Rb and Cs take a "corner" configuration with  $\text{H}_2\text{O}$ –AM– $\text{OH}_2$  angle  $\sim 100^\circ$ , while it takes a straight configuration ( $\text{H}_2\text{O}$ –AM– $\text{OH}_2$  angle =  $180^\circ$ ) for Li, Na, and K. Similar trends appear in gas phase shells.<sup>35</sup>

### C. Interaction between hydrated ions

In order to study the (screened) interaction between (hydrated) ions and its influence on ion hydration at the surface, we investigate ion hydration at higher ion coverages on graphite (0001). For bare two to four ions adsorption on the graphite [coverage  $\sim (2.4\text{--}2.48) \times 10^{14}$  atoms/ $\text{cm}^2$ ], adsorption energies and ion separations are calculated, as shown in Table IV. The ions deviate from exact hollow sites. The equilibrium ion-ion separation of an adsorbed dimer is 3.27 Å for  $\text{Na}_2$  and 4.90 Å for  $\text{K}_2$ , with adsorption energies of 0.797 and 0.856 eV per ion, respectively. Compared with atomic distances in bulk body-centered-cubic (bcc) metals, the K–K separation at surface is larger than that in bulk (4.61 Å), while the Na–Na is shorter than in bcc Na (3.72 Å). The interaction between adsorbed ions also introduces an elongation of the ion-surface separation at the level of 0.3–0.6 Å. Adsorption of three and four ions has similar behaviors to an

TABLE V. Hydration energies ( $E_h$ ), distances ( $d$ ), and ion coordination numbers (CN) for the hydration of a K dimer ( $\text{K}_2$ ) with  $n$   $\text{H}_2\text{O}$  on graphite surface. Energies in eV and distances in angstrom.

$n$	$E_h$	$d_{\text{K-K}}$	CN( $\text{K}^1$ )	$d_{\text{K1-S}}$	CN( $\text{K}^2$ )	$d_{\text{K2-S}}$
1	0.581	4.324	1	3.007	1	3.008
5	0.590	4.956	3	3.094	3	3.754
10	0.598	4.733	3	3.015	3	5.609

ion dimer. The larger K–K separation and smaller Na–Na separation indicate the clustering behavior of Na ions is favored, while K has less interaction between each other. This is further evidenced by the change in adsorption energies. Many Na adsorption *enhances* the Na adsorption energy to 0.05–0.16 eV/ion higher than single Na; in contrast, the K–K interaction *lowers* the adsorption energy by 0.07–0.14 eV/ion, indicating a repulsive interaction between K ions.

We next study the hydration of the adsorbed ion clusters on graphite. Structures and energies for several representative systems, i.e., an ion dimer coadsorbed with one, five, and ten  $\text{H}_2\text{O}$  molecules, are listed in Tables V and VI. The separation of K (Na) is around 4.3–4.9 Å (3.3–3.6 Å) after hydration, in the same range as bare ion adsorption. This suggests the ion-ion interaction is little perturbed by the hydration process. However, the hydration affects the ion-surface separation much. One of the K ion in the dimer is lifted from the height of 3.0–5.6 Å, from  $\text{K}_2 + 1\text{H}_2\text{O}$  to  $\text{K}_2 + 10\text{H}_2\text{O}$  cases, while the other K remains at 3.0 Å above the surface. This is also true for the Na case, where two Na-surface distances  $\geq 4.0$  Å in the system  $\text{Na}_2 + 10\text{H}_2\text{O}$ . In both K and Na cases, the hydration energy is around 0.6 eV/ $\text{H}_2\text{O}$ , in agreement with single ion hydration.

The clustering behavior of Na on the graphite surface is retained after water hydration. Na ions prefer to aggregate and make bonds directly with each other, while the interaction between K ions is mediated by the shared water molecules. For example, water tends to bond only one of the Na in the  $\text{Na}_2$  dimer; on the contrary, water sits between two K in  $\text{K}_2$  making two O–K bonds. The K–K distance is shortened by 0.6 Å through the mediation of the  $\text{H}_2\text{O}$  molecule. MD simulations of  $\text{K}_2$  and  $\text{Na}_2$  dimers with ten  $\text{H}_2\text{O}$  at 85 K have confirmed this picture. Na is easy to aggregate with an averaged distance of 3.58 Å, while K is always separated by 5.50 Å on average during the 4 ps trajectory. Similar behavior is expected for systems consisting of three to four ions plus several waters.

The aggregation nature of Na ion on graphite seems to be unique among Li, Na, K, Rb, and Cs. This is due to the weakest bond strength between Na and graphite, as shown in Table I. Among AM studied here, only the adsorption energy

TABLE VI. Same as Table V but for a Na dimer ( $\text{Na}_2$ ).

$n$	$E_h$	$d_{\text{Na-Na}}$	CN( $\text{Na}^1$ )	$d_{\text{Na1-S}}$	CN( $\text{Na}^2$ )	$d_{\text{Na2-S}}$
1	0.595	3.326	1	3.023	0	3.330
5	0.613	3.591	4	2.937	3	4.249
10	0.619	3.529	5	4.701	4	3.994

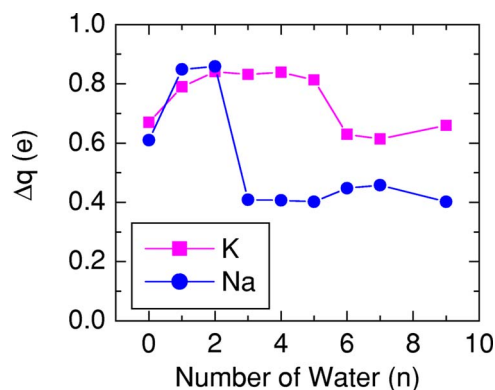


FIG. 6. (Color online) The charge transfer from K (squares) and Na (dots) ion to the graphite surface, in a hydration shell with  $n$  water molecules.

of Li and Na is less than the corresponding cohesive energy in bulk bcc metals, which is 1.65, 1.11, 0.92, 0.84, and 0.79 eV for Li, Na, K, Rb, and Cs, respectively. Stronger ion-ion attraction than the surface bind energy would favor ion clustering. From the adsorption and hydration energetics we obtained, we could infer that Rb, Cs behaves like K, while Li aggregation might be suppressed by a relatively large diffusion barrier ( $\sim 0.3$  eV, estimated by the energy difference between the hollow site and top site) at a low temperature as 85 K. The aggregation behavior of Na at the water-graphite interface, in contrast with Li, K, Rb, and Cs, agrees with the experimental EELS observation.<sup>11,17</sup>

In experiments, large amount of AM adsorption above a critical coverage could introduce chemical reactions forming hydroxides. However, from our simulation on  $K_2+10H_2O$  and  $Na_2+10H_2O$  at 85 K we did not observe any water dissociation during the 4 ps long trajectory. In fact the  $Na_2+OH+H$ /graphite configuration is less stable by 2.4 eV than intact  $H_2O$  adsorption.

#### D. Dynamical charge transfer during hydration

Charge density analysis shows a strong size-dependent electron transfer from adsorbates to the surface involved in the hydration process. Figure 6 presents number of electrons transferred from K and Na hydration shells to graphite. Charge transfer has been estimated by integrating the K 4s (or Na 3s) electron density in the thin region from  $-1.75$  to  $1.75$  Å above the graphite sheet ( $\Delta z = \pm 1.75$  Å). Free K is more ionized than Na on graphite, losing  $0.68e$  ( $0.61e$  for Na) to the surface. This is consistent with the DOS and charge plot in Figs. 1 and 2. In the initial stage of ion hydration (with  $n=1-2$  waters) more electrons are transferred to the surface than single ion adsorption, either through enhanced ionization or indirect electron transfer from  $H_2O$ . This trend is kept when more water is added to the K shell. However, charge transfer is significantly reduced to  $\sim 0.4e$  when more waters added to the Na shell, due to the large separation between the Na and the surface. From Table III, it is shown that Na ion is lifted from the surface by water at  $n \geq 3$ . This agrees well with experimental estimations that K and Na is partially ionized of  $0.6e$  and  $0.3e$  by the surface, respectively, at high water coverages (three to four  $H_2O$  per

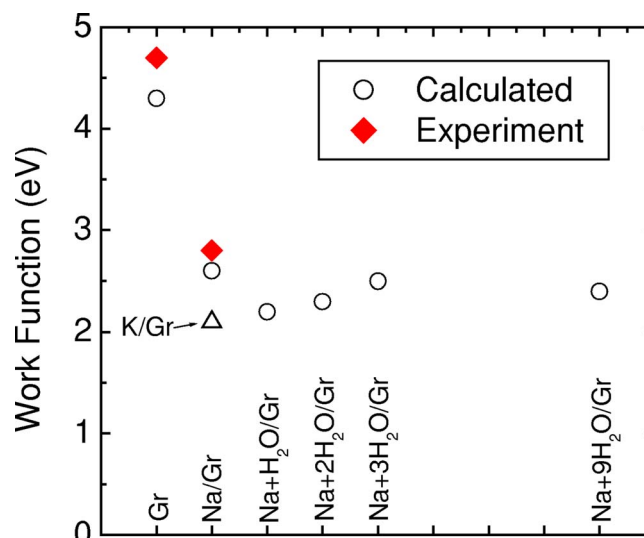


FIG. 7. (Color online) Calculated work functions of graphite (0001) surface upon Na and water adsorption (circles), and K adsorption (triangle). Diamonds show the experimental data (Ref. 18).

AM).<sup>10,11</sup> Such a dynamical charge effect, which is general to all ionic processes at surfaces, can only be handled to sufficient accuracy in *ab initio* simulations.

To verify the above picture, we point out surface charge transfer is strongly related to work function change upon adsorption, which is a measurable quantity. As simple electrostatic calculation indicates, the work function change  $\Delta\Phi$  is directly related to the change in the surface dipole. In many cases (e.g., in the absence of adsorbate induced multipoles<sup>36</sup>), the simple dipole-charge transfer relationship holds, so

$$\Delta\Phi = \frac{\Delta q_a d \theta_a}{4\pi\epsilon_0}. \quad (3)$$

Here  $\Delta q_a$  is the charge transfer induced by the adsorbate along surface normal,  $d$  is the mean distance of charge separation in the dipole layer and  $\theta_a$  is the adsorbate coverage. Figure 7 shows the calculated work functions of the bare graphite surface, the graphite with K and Na adsorptions, and with Na hydration clusters. Comparing work function data with the charge transfer in Fig. 6, suggests a close correlation between them. One notes that Na adsorbate significantly reduces surface work function from 4.3 to 2.6 eV, due to the large charge transfer ( $0.61e$ ) Na introduces to the graphite. K reduces it further to 2.1 eV, because of even larger charge transfer. However, coadsorption with water in certain coverages, does not change the work function significantly. The work function is around 2.4 eV for  $Na+nH_2O$  as  $n$  grows from 1 to 9, because the height of HS increases and therefore the induced dipole is kept almost constant. The available experimental data for bare graphite and that with Na adsorbed at the same coverage, are also drawn in Fig. 7, which read 4.5 and 2.8 eV, respectively.<sup>18</sup> The close match between theoretical and experimental data confirms again that the charge transfer effect is captured correctly by our first-principles models.

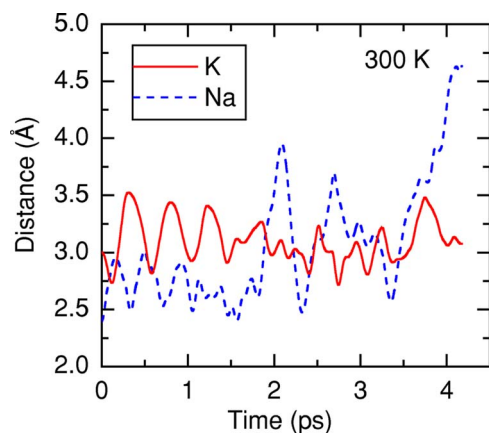


FIG. 8. (Color online) The ion-surface distance as a function of simulation time at the interface of graphite and bulk water.

### E. Dynamics of the hydration shells at the liquid water/graphite interface

Increasing water coverage further beyond the finite-size cluster regime results in water multilayer formation on the surface, and finally reaches liquid water/graphite interface at the bulk water limit. The hydration structure and dynamics at the liquid-solid interface differs significantly from that at low water coverages. For example, a variety of ion species are dissolved by the presence of liquid water while others bind on the solid surface. The latter, so deemed as “sticky” ions, are immensely useful in crystal growth, catalysis, electrolysis, environmental protection, and signal transport.<sup>37</sup>

We simulate the liquid water/graphite interface by inserting 37 H<sub>2</sub>O between the adjacent graphite sheets, to achieve a water density of  $\sim 1$  g/cm<sup>3</sup>. The initial configuration of water was taken from classical and subsequent *ab initio* MD simulations of bulk water at 300 K. Water molecules around the ion and close to the interface were subject to modification to make appropriate H<sub>2</sub>O-ion and H<sub>2</sub>O-surface contacts. In the starting configurations, the ions were put in their equilibrium positions on graphite as on bare surface. Separate molecular dynamics simulations of K and Na at the interface have been performed at a constant temperature of 300 K with a time step of 0.5 fs. After equilibrating the system by 1 ps, the trajectories lasting  $>4$  ps long were collected for analysis.

Figure 8 shows the ion-surface distances during the simulation. The K ion stays at the interface all the time at an equilibrium ion-surface distance of 3.2 Å and does not dissolve. In contrast, the average Na-surface distance increases significantly along the simulation from its equilibrium around 2.6 Å to larger than 5 Å. Near the end of the simulation, the Na ion is solvated into liquid water completely. This shows a contrasting behavior between K and Na at the water-graphite interface. K always presents at surface while Na is dissolved. This is consistent with the picture that K is a sticky ion which breaks the hydrogen bond network between water molecules while Na is a “structure former” in water.<sup>37</sup> Interestingly, it also resembles the well-established concept that larger Cl<sup>-</sup> presents at the air/water interface while F<sup>-</sup> goes to interior of a water drop.<sup>38</sup> We have also estimated the diffusion coefficient of H<sub>2</sub>O and ions by ana-

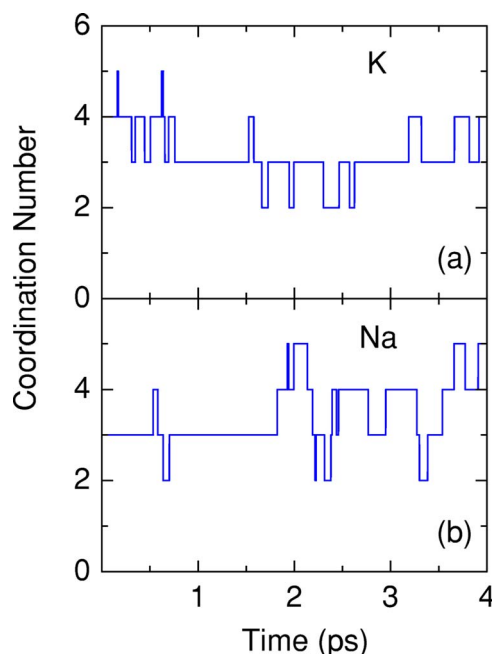


FIG. 9. (Color online) The coordination number of the K and Na ion as a function of simulation time at the water/graphite interface.

lyzing their mean square displacement during the simulation. Water has a diffusion coefficient of 0.21 Å<sup>2</sup>/ps, agrees with other *ab initio* result of 0.22 Å<sup>2</sup>/ps,<sup>39</sup> and experimental value of 0.24 Å<sup>2</sup>/ps.<sup>40</sup> K and Na ions have different diffusion coefficients of 0.17 and 0.33 Å<sup>2</sup>/ps, respectively. However, the large apparent diffusion coefficient of Na may come from increasing heights above graphite due to the short simulation time and initial conditions.

The remarkable difference between K and Na at the graphite-water interface is attributed to the competition between ion hydration and ion-surface interaction. As discussed before, Na atom has the stronger hydration force and smaller binding energy to the surface than K due to its smaller ionic radii and larger electronegativity. Therefore the hydration force wins in the Na case, dissolving Na into liquid water. This is evidenced by the variation in coordination number (CN) of the ions, shown in Fig. 9. CN is defined by the number of water molecules in the first hydration shell, which has the radius of 3.2 Å for K and 2.9 Å for Na, according to the first minimum in the pair correlation functions of  $g_{OK}$  and  $g_{ONa}$ .<sup>15</sup> One notes that the CN of K is around 3 all the time, while the CN of Na increases from 3 to 4–5 gradually along its dissolution trajectory, after which it is exposed to more water molecules where the mechanical confinement of the surface diminishes. It is worth to mention that the more stable HS of Na is believed to play a key role in the selectivity of ion channels,<sup>41</sup> where the energy cost for depriving the hydration shell competes sensitively with the energy gain when entering the channels.

Very interestingly, K binds to the surface and retains its hydration shell structure at the water/graphite interface, just as that at low water coverages. This adds further evidence to the belief that K is a “water-structure breaker,” in complementary with the thermodynamic, transport, spectroscopic, and diffraction data in experiments.<sup>37</sup> We refer the K hydration shell, which is stable at the solid-water interface, as a

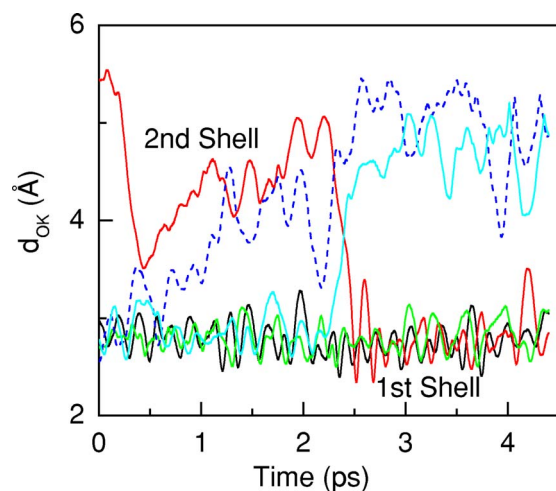


FIG. 10. (Color online) The O–K distances in the first hydration shell of K as functions of simulation time. K accommodates three H<sub>2</sub>O in the first shell on average. Dashed line shows the H<sub>2</sub>O in the second hydration shell perturbs into the first shell temporarily (the first 0.5 ps).

surface hydration shell, which differs from the 3D hydration shells in bulk water and gaseous clusters.<sup>35</sup>

It is thus important to explore the structural and dynamical properties of the surface hydration shell identified in the K+water/graphite system. The O–K distances in the shell are plotted as a function of simulation time in Fig. 10. There is a clear separation between the first HS and the second HS. The O–K distances in the first HS oscillate around 2.8 Å with a vibration period of ~150 fs, while those in the second HS has a looser structure with O–K distances >4.5 Å. Exchange of water molecules between the first and the second HS is observed at a time interval of 2.1–2.5 ps. At time  $t=2.3$  ps, a H<sub>2</sub>O in the first HS leaves K, while another H<sub>2</sub>O originally in the second HS fits in promptly within 0.4 ps, indicating the first shell is rather rigid. The H<sub>2</sub>O molecules in the second HS could also perturb into the first shell temporarily (dashed line), resulting in CN oscillations in Fig. 9. However, in Fig. 10, it is clearly shown that K surface HS accommodates three water molecules on average.

Figure 11 shows the geometrical characteristics of the surface HS with respect to the surface plane. The angular distribution of the H<sub>2</sub>O–K–surface angle is calculated from the 4 ps simulation trajectory, and averaged over all the water molecules in the first HS. The maximum of the distribution locates at the O–K–surface angle of 115°, suggesting K forms an umbrellalike shell on the graphite surface (Fig. 11 insert). In this structure, the average O–K–O angle between the water molecules is 95°. Both angles deviate from the ideal tetrahedral angle 109.5° as for the O–K–O in solutions, due to the presence of the surface. These angles might have a minimal dependence on temperature, because the determinative factors—the surface-K and K-water interactions—are less affected by the temperature. Although demonstrated on the model system of K/graphite, the unique umbrella structure could sustain at other solid-liquid interfaces, serving as a possible model for sticky ions at interface.

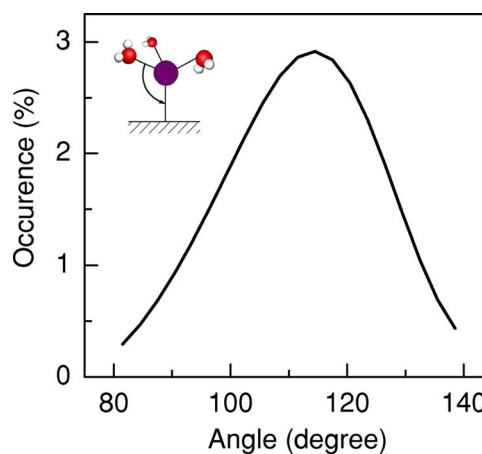


FIG. 11. (Color online) Angular distribution of the H<sub>2</sub>O–K–surface angle at the water/graphite interface at 300 K. K stays at the graphite surface, forming an umbrellalike surface hydration shell with three H<sub>2</sub>O in the first shell (insert).

#### IV. CONCLUSIONS

*First success of the hard problem.* As discussed in Sec. II, there have been encountered several severe difficulties in the present-day theoretical treatments of ion hydration at water/graphite interface, such as accurate potentials between ion, water, and the surface, magnificent charge transfer, substrate relaxation, and finite supercell size effects. Despite these difficulties, we have shown in this work the first successful results towards this hard problem, evidenced by consistence with experimental measurements and other theoretical models (different pseudopotentials and XC functionals). Some sacrifices have to be paid in our treatment of water/graphite interface employing *ab initio* MD simulations and slab models with periodical boundary conditions. For instance, the vdW interaction evolved is neglected, and simulation period is short. How the neglected interaction, the short simulation time, the finite cell size, and the temperature effect will influence the formation and interaction of surface hydration shells would be important in future studies. To summarize our first results towards a complete description of the ion hydration at interfaces, our conclusions are

- (i) All the AM ions studied here, Li, Na, K, Rb, and Cs, bind to the graphite (0001) surface on hollow sites, partially ionized. Na has the weakest bonding to graphite.
- (ii) At low water coverages, AM ions form hydration shells that are different from gas phase. The HS at surface are flat, two-dimensional, due to the mechanical confinement of the surface.
- (iii) Li and Na accommodate four water molecules in the first shell, while K, Rb, and Cs have at most three. This is also confirmed by comparison between the calculated and experimental vibration spectra.<sup>16</sup>
- (iv) Higher coverage of alkali metals introduces ion-ion interactions. Na prefers to aggregate upon hydration, while Li, K, Rb, and Cs does not, due to either the kinetic constrain or thermodynamics. Instead, the ion-ion interaction in the latter is screened by water.
- (v) Most interestingly, the competition between hydration

and ion-surface interaction at high water coverages, leads to Na dissolution into liquid water. The K ion, on the contrary, preserves at the liquid water/graphite interface, rendering an “umbrellalike” surface hydration shell.

- (vi) Finally, the dynamical charge transfer associated with the structural transformation agrees with measured work function data, implying the essential to describe surface ion hydration from electronic structures.

## ACKNOWLEDGMENTS

The authors acknowledge insightful discussions with Professor B. Kasemo, Professor D. Chakarov, Professor B. Lundqvist, Professor E. G. Wang, Professor M. Sprik, and Professor M. Tuckerman. This work is partially supported by U.S. NSF (Grants Nos. DMR-0306239 and DMR-0325218) and DOE (Grant No. DE-FG03-02ER45958), and the Swedish Research Council (VR) through VR 621-2001-2614. ORNL is managed by UT-Battelle, LLC, for the DOE under Contract No. DE-AC05-00OR22725.

<sup>1</sup>P. A. Thiel and T. E. Madey, *Surf. Sci. Rep.* **7**, 211 (1987).

<sup>2</sup>M. A. Henderson, *Surf. Sci. Rep.* **46**, 1 (2002).

<sup>3</sup>B. Kasemo, *Surf. Sci.* **500**, 656 (2002).

<sup>4</sup>S. Ghosh, A. K. Sood, and N. Kumar, *Science* **299**, 1042 (2003).

<sup>5</sup>G. E. Brown, V. E. Henrich, W. H. Casey *et al.*, *Chem. Rev. (Washington, D.C.)* **93**, 77 (1999).

<sup>6</sup>H. Bayley and P. S. Cremer, *Nature (London)* **413**, 226 (2001).

<sup>7</sup>H. Ohtaki and T. Radnal, *Chem. Rev. (Washington, D.C.)* **93**, 1157 (1993).

<sup>8</sup>Y. Marcus, *Chem. Rev. (Washington, D.C.)* **88**, 1475 (1988).

<sup>9</sup>H. P. Bonzel, G. Pirug, and J. E. Müller, *Phys. Rev. Lett.* **58**, 2138 (1987).

<sup>10</sup>D. V. Chakarov, L. Österlund, and B. Kasemo, *Langmuir* **11**, 1201 (1995).

<sup>11</sup>M. A. Gleeson, K. Martensson, B. Kasemo, and D. V. Chakarov, *Appl. Surf. Sci.* **235**, 91 (2004).

<sup>12</sup>M. Odelius, M. Bernasconi, and M. Parrinello, *Phys. Rev. Lett.* **78**, 2885 (1997).

<sup>13</sup>L. Cheng, P. Fenter, K. L. Nagy, M. L. Schlegel, and N. C. Sturchio,

*Phys. Rev. Lett.* **87**, 156103 (2001).

<sup>14</sup>S. Izvekov and G. A. Voth, *J. Chem. Phys.* **115**, 7196 (2001).

<sup>15</sup>L. M. Ramaniah, M. Bernasconi, and M. Parrinello, *J. Chem. Phys.* **111**, 19587 (1999).

<sup>16</sup>S. Meng, D. V. Chakarov, B. Kasemo, and S. W. Gao, *J. Chem. Phys.* **121**, 12572 (2004).

<sup>17</sup>D. V. Chakarov and B. Kasemo (private communication).

<sup>18</sup>M. Pivetta, F. Patthey, I. Barke, H. Hovel, B. Delley, and W. D. Schneider, *Phys. Rev. B* **71**, 165430 (2005).

<sup>19</sup>G. Kresse and J. Hafner, *Phys. Rev. B* **47**, 558 (1993).

<sup>20</sup>D. Vanderbilt, *Phys. Rev. B* **41**, 7892 (1990).

<sup>21</sup>J. P. Perdew, J. A. Chevary, S. H. Vosko, K. A. Jackson, M. R. Pederson, D. J. Singh, and C. Fiolhais, *Phys. Rev. B* **46**, 6671 (1992).

<sup>22</sup>P. E. Blöchl, *Phys. Rev. B* **50**, 17953 (1994).

<sup>23</sup>J. P. Perdew, K. Burke, and M. Ernzerhof, *Phys. Rev. Lett.* **77**, 3865 (1996).

<sup>24</sup>S. Tsuzuki and H. P. Lüthi, *J. Chem. Phys.* **114**, 3949 (2001).

<sup>25</sup>D. R. Hamann, *Phys. Rev. B* **55**, R10157 (1997).

<sup>26</sup>J. VandeVondele, F. Mohamed, M. Krack, J. Hutter, M. Sprik, and M. Parrinello, *J. Chem. Phys.* **122**, 014515 (2005).

<sup>27</sup>S. Kurth, J. P. Perdew, and P. Blaha, *Int. J. Quantum Chem.* **75**, 889 (1999).

<sup>28</sup>Z. H. Zhu, G. Q. Lu, and F. Y. Wang, *J. Phys. Chem. B* **109**, 7923 (2005).

<sup>29</sup>L. X. Beredict, N. G. Chopra, M. L. Cohen, A. Zettl, S. G. Louie, and V. H. Crespi, *Chem. Phys. Lett.* **286**, 490 (1998).

<sup>30</sup>N. Lamoén and B. N. Persson, *J. Chem. Phys.* **108**, 3332 (1998).

<sup>31</sup>N. N. Avgul and A. V. Kiselev, in *Chemistry and Physics of Carbon*, edited by P. L. Walker (Dekker, New York, 1970), Vol. 6.

<sup>32</sup>S. Siraci, S. Dag, T. Yildirim, O. Gülseren, and R. T. Senger, *J. Phys.: Condens. Matter* **16**, R901 (2004).

<sup>33</sup>A. Sandell, O. Hjortstam, A. Nilsson, P. A. Bruhwiler, O. Eriksson, P. Bennich, P. Rudolf, J. M. Wills, B. Johansson, and N. Martensson, *Phys. Rev. Lett.* **78**, 4994 (1997).

<sup>34</sup>H. H. Loeffler and B. M. Rode, *J. Chem. Phys.* **117**, 110 (2002).

<sup>35</sup>O. Borodin, R. L. Bell, Y. Li, D. Bedrov, and G. D. Smith, *Chem. Phys. Lett.* **336**, 292 (2001).

<sup>36</sup>A. Michaelides, P. Hu, M. H. Lee, A. Alavi, and D. A. King, *Phys. Rev. Lett.* **90**, 246103 (2003).

<sup>37</sup>K. D. Collins, *Proc. Natl. Acad. Sci. U.S.A.* **92**, 5553 (1995).

<sup>38</sup>P. Jungwirth and D. J. Tobias, *J. Phys. Chem. B* **106**, 6361 (2002).

<sup>39</sup>K. Laasonen, M. Sprik, M. Parrinello, and R. Car, *J. Chem. Phys.* **99**, 9080 (1993).

<sup>40</sup>K. Krynicky, C. D. Green, and D. W. Sawyer, *Faraday Discuss. Chem. Soc.* **66**, 199 (1978).

<sup>41</sup>D. A. Doyle, J. M. Cabral, R. A. Pfuetzner, A. L. Kuo, J. M. Gulbis, S. L. Cohen, B. T. Chait, and R. MacKinnon, *Science* **280**, 69 (1998).